CHAPTER 14

Cellulose and Protein Aerogels for Oil Spill Cleaning, Life Science and Food Engineering Applications

HAI M. DUONG,* PENG LIU, THANH X. NGUYEN, SON T. NGUYEN, JINGDUO FENG AND HANLIN CHENG

Department of Mechanical Engineering, National University of Singapore, 9 Engineering Drive 1, EA-07-05, Singapore 117575, Singapore
*Email: mpedhm@nus.edu.sg

14.1 Introduction

Oil spills are considered to be one of the most serious disasters threatening the marine ecosystem. Recently, the explosion of a drilling rig in the Gulf of Mexico caused significant environmental damage.[1] Oil spills are usually related to accidents during oil production, storage, and transportation. As long as fossil fuels are needed, oil spills will remain a significant problem that human beings will have to face.[2–8] Therefore, it is essential to solve, or at least alleviate, this environmental problem.

Several methods of oil spill–cleaning have been developed, and can be classified as chemical, biological, and physical methods. Dispersion, *in situ* burning, and solidification are considered to be chemical methods that are complicated and expensive.[9–11] The use of microorganisms *via* biological

Green Chemistry Series No. 58
Biobased Aerogels: Polysaccharide and Protein-based Materials
Edited by Sabu Thomas, Laly A. Pothan and Rubie Mavelil-Sam

Published by the Royal Society of Chemistry, www.rsc.org

methods is effective but requires a long time, and the microorganisms are affected by environmental factors, such as pH, temperature, and oxygen content.[12] Moreover, oil spills cleaned using chemical and biological methods are difficult to recover, and recoverability is a crucial factor for oil spill–cleaning applications. With regards to the physical methods, booms and skimmers are often used, but cannot remove oil from the sea effectively.[13] Of these methods, sorption has been considered one of the most effective ways for oil-spill cleaning, as it enables the collection and complete removal of oil from oil-spill sites.[2,11,14–20]

Several materials have been used as sorbents for oil-spill cleaning in both research and practical applications. The oil absorbents can be categorized into inorganic minerals, natural organic materials, and synthetic organic materials.[11,16,17,19] Inorganic materials, such as clay, vermiculite, exfoliated graphite, diatomite, and fly ash, have low oil absorption capacities (4–20 $g\,g^{-1}$).[21–23] Furthermore, some of these inorganic materials, such as clay and vermiculite, are harmful when inhaled by human beings under windy conditions, due to the loose structures of these materials. Natural organic materials from plant and animal residues, such as kapok fibre, sugar-cane bagasse, rice husk, coconut husk, cotton, wool, sawdust, and chitosan, have been examined for oil absorption capabilities.[24–26] However, most of the materials have low oil absorption abilities (3–15 $g\,g^{-1}$), and also absorb water.

On the other hand, synthetic organic materials, such as polypropylene, polystyrene, and polyurethane, possess a high affinity with oil and high oil absorption capacities (4.5–100 $g\,g^{-1}$), but cause waste problems after use due to their slow rates of degradation.[11,16,19] Therefore, there is high demand for new environmentally friendly absorbents with a high oil absorption capacity, good selectiveness, and low cost for oil-spill removal.

A combination of an aerogel structure and recycled cellulose fibres from paper waste can be used to form an advanced material, called a recycled cellulose aerogel, which is cost-effective and a promising material for oil absorption. Although some studies have investigated the use of cellulosic materials for oil absorption, none have fabricated aerogels from paper-waste cellulose fibres and investigated them as absorbents for crude oil-spill cleaning.[2,5,27–31]

The increase in paper consumption has created huge amounts of paper waste, which accounts for 25–40% of global municipal solid waste.[32] In 2004 alone, 360 million tonnes of paper-related waste was generated worldwide. Moreover, paper and paperboard consumption will increase the amount of waste produced by 2.1% each year until 2020, which suggests that more than 500 million tonnes of paper waste can be expected in 2020.[33] In addition, incineration or landfill of the paper waste could damage the environment further with toxic emissions and groundwater contamination.

Recycling paper waste will help to preserve forests and solve the environmental problem. Therefore, it is important to recycle or convert this enormous amount of waste into useful products. Several efforts have been

made to solve this problem. For instance, in 2010, 63% of paper waste was recycled in the US.[34] Paper waste has also been investigated as a raw material for production of bioethanol, polymer precursors, particleboard, and so forth.[32,35,36] Commercially, recycled paper is mainly converted into other paper commodities of lower quality grades than the original products.[37] In addition, the maximum conversion rate from paper waste to other paper products is only approximately 65%.[37] This low conversion rate is due to the length degradation of the cellulose fibres during the recycling processes, which also compromises the quality of the end product.[37] In addition, waste fibres of short lengths generated during recycling are discarded, as they are not suitable for further recycling.[37] It is therefore necessary to develop alternative commodities from paper waste. Although some studies have examined the use of cellulosic materials for oil absorption, none have covered the fabrication of aerogels from paper-waste cellulose fibres, and investigated the aerogels as absorbents for the cleaning of crude-oil spills.[2,5,27–31]

Recycled cellulose fibres from paper waste are a cheap and abundant resource; the price of scrap paper was approximately $100/ton in 2015.[38] A combination of the aerogel structure and recycled cellulose fibre constitute a new material – called a recycled cellulose aerogel – which is cost-effective and has the potential for oil absorption.[39–41] The recycled cellulose aerogel and its silica composite aerogel can also potentially be used as thermal-insulation materials for buildings.[41] Therefore, all the practical applications developed may contribute to the recycling of paper-related waste. This book chapter presents the basic facts about cellulose materials, and comprehensive information about cellulose aerogels and silica–cellulose composite aerogels. Both the fabrication methods and properties of cellulose aerogels and silica–cellulose aerogels are discussed in detail.

In recent years, the production of natural protein-based aerogels has become a highly attractive subject in materials chemistry due to the requirement of biodegradability and biocompatibility for pharmaceutical, medical and food applications.[42] Several types of proteins, including whey protein,[43–45] silk fibroin,[46,47] egg white protein[48] and soy protein,[49–52] have been exploited for the formation of aerogels. The effects of various synthesis conditions, such as drying methods,[43] pH values,[48] ionic strengths[48] and precursor concentrations[47] have been investigated for optimizing the porous structure and multi-properties of the resultant aerogels. These natural aerogels are promising as drug carriers and encapsulation materials.

14.2 Recycled Cellulose Aerogels Using Kymene Binder for Oil Spill–Cleaning Applications

14.2.1 Introduction

This section describes the successful development of an advanced and cost-effective method for the fabrication of recycled cellulose aerogels.

This novel method synthesizes the recycled cellulose aerogels from paper waste by using Kymene as a cross-linker, instead of using sodium hydroxide and urea as in previous reports.[53–55] This method can significantly reduce the toxicity of raw materials, and reduce the entire synthesis duration fromnine days, as in previous methods, to three days.[40,41] After being freeze dried and coated with methyltrimethoxysilane (MTMS) *via* chemical vapour deposition, the recycled cellulose aerogels exhibited ultra-flexibility, high porosity, super-hydrophobicity, and outstanding oil absorption capability.

14.2.2 Synthesis of Cellulose Aerogels Using a Kymene Binder

Recycled cellulose fibres were directly purchased from the market because the established raw–paper waste recycling methods are mature, and using commercial recycled cellulose fibres is cost-effective and time-saving. The recycled cellulose fibres from paper waste (0.075–0.3 g) and Kymene (5–20 μl) were first dispersed in 30 ml of DI water by sonicating the mixtures for 10 min. The suspensions were then placed in a refrigerator at −18 °C for more than 12 h to allow the gelation. The cellulose aerogels were obtained by freeze drying the obtained gels at −98 °C for two days using a Scan Vac CoolSafe 95-15 Pro freeze dryer (Denmark). Thereafter, the cellulose aerogels were further cured at 120 °C for another 3 h to completely cross-link the Kymene molecules.

As the development of the recycled cellulose aerogels was hydrophilic, the highly porous networks of the as-prepared cellulose aerogels were coated with MTMS, to form super-hydrophobic cellulose aerogels for oil absorption and thermal insulation. The proposed coating mechanism[53,54] of the silanation reaction between the cellulose and MTMS is illustrated in Figure 14.1.

The cellulose aerogels and open glass vials containing MTMS (0.5 ml) were placed in big containers. The containers were then capped and heated at 70 °C for 3 h for the silanation reaction. After the aerogel structure was coated completely, excessive MTMS was removed by placing the aerogel in a vacuum oven until the pressure decreased to below 0.03 mbar.

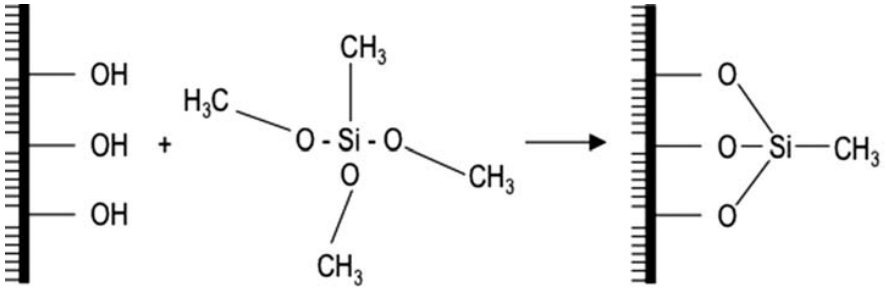

Figure 14.1 The proposed silanation reaction between cellulose and MTMS, which results in super-hydrophobic cellulose aerogels.

14.2.3 Morphology and Hydrophobicity of the Recycled Cellulose Aerogels

In this section, the morphologies and hydrophobic properties of the recycled cellulose aerogels are discussed. The recycled cellulose aerogels exhibited macropore structures. Moreover, the aerogel with the higher cellulose concentration (1.0 wt.%) had a more compacted network and lower porosity. The aerogel with a high stability was also observed to have super-hydrophobicity.

14.2.3.1 Effects of the Cellulose Concentrations

The photographs and SEM images of the developed recycled cellulose aerogels are shown in Figure 14.2. The aerogel sample in Figure 14.2a had dimensions of 45 mm (diameter)×11 mm (thickness), and the same shape as that of its reaction container. As reported previously, the recycled cellulose aerogels were formed *via* hydrogen bonding between the self-assembled cellulose fibres.[40,54]

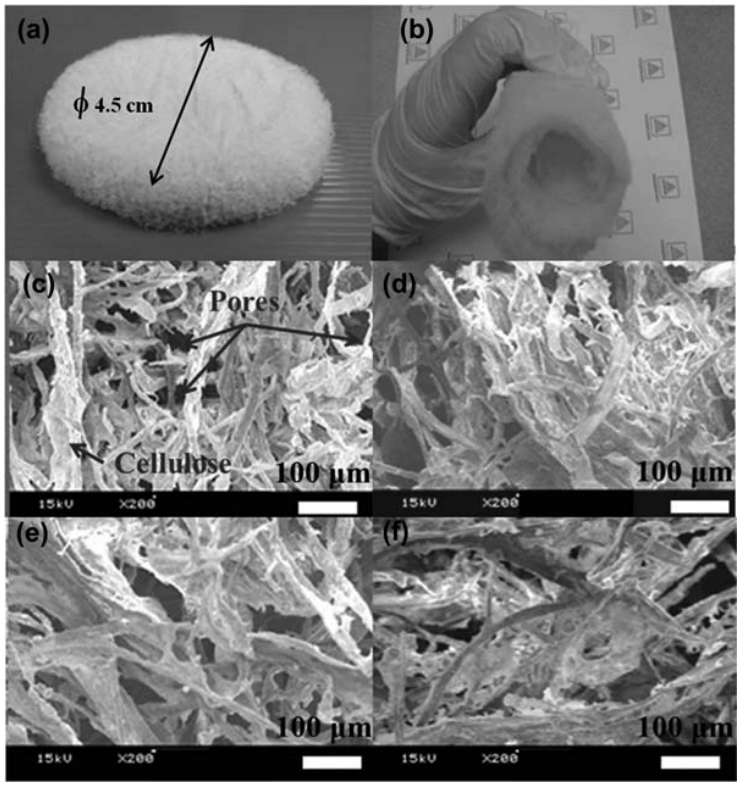

Figure 14.2 (a) Super-hydrophobic recycled cellulose aerogel. (b) Flexibility of the large-scale cellulose aerogel (38 cm×38 cm×1 cm) containing 0.60 wt.% of cellulose fibres, SEM images of the cellulose aerogels with different ratios of cellulose fibres (wt.%) and Kymene (µl): (c) 0.25:5, (d) 1.00:5, (e) 0.60:5, and (f) 0.60:20.
(Reprinted from *Chemical Engineering Journal*, **270**, J. Feng, S. T. Nguyen, Z. Fan, H. M. Duong, Advanced fabrication and oil absorption properties of superhydrophobic recycled cellulose aerogels, 168–175, Copyright 2015,with permission from Elsevier).

In addition, Kymene strengthened the cellulose aerogels by providing a protection mechanism and reinforcement mechanism.[56] For the protection mechanism, some Kymene molecules reacted with other Kymene molecules, and the formed Kymene networks wrapped the cross-linking points between the cellulose fibres to improve the strength of the cellulose network.[56] Moreover, Kymene molecules also bonded with the cellulose fibres to enhance the strength of the cellulose network, providing the reinforcement mechanism.[56] The utilization of Kymene as a cross-linker ensured that the resultant aerogels had a robust structure.[56]

In contrast to the mesopores (2–70 nm) of the aerogels formed by the cellulose nanofibres, the cellulose aerogels with macropores (>50 nm) had a highly porous structure, which can be clearly observed in the SEM images in Figure 14.2c–f.[57–59] Their macropores were possibly caused by the larger size of the recycled cellulose fibres, obtained from the paper waste.[40] Figure 14.2c and d show the morphologies of the cellulose aerogels with cellulose concentrations of 0.25 and 1.00 wt.%, respectively. The aerogel with the higher cellulose concentration (1.0 wt.%) had a more compacted network and lower porosity. However, an increase in the amount of Kymene from 5 to 20 μl in a 30 ml reaction mixture did not significantly impact the aerogel structures, as shown in Figure 14.2e and f, as the amount of Kymene was small compared to that of the cellulose fibres, and the possible minor structure changes might not have been observed.

14.2.3.2 Hydrophobicity of the Cellulose Aerogels

In order to investigate the super-hydrophobicity of the developed cellulose aerogels, the water contact angles were measured on both the external surface and the cross-section of the MTMS-coated cellulose aerogels. As shown in Figure 14.3a and b, large contact angles of 153.5° and 150.8°, respectively, were obtained, thus proving that the hydrophobic coating successfully covered the whole aerogel network. The water contact angle

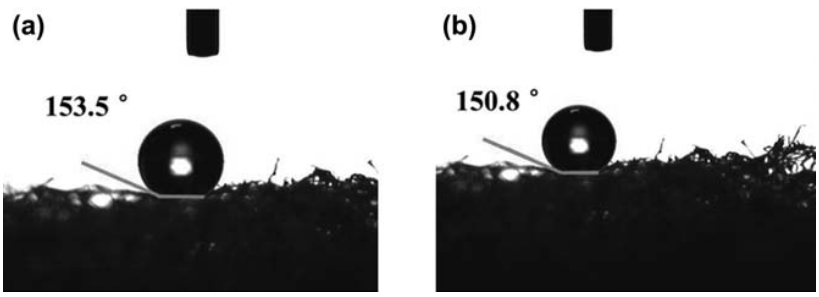

Figure 14.3 Water contact angles on (a) the external surface and (b) the cross-section of the super-hydrophobic recycled cellulose aerogel. (Reprinted from *Chemical Engineering Journal*, **270**, J. Feng, S. T. Nguyen, Z. Fan, H. M. Duong, Advanced fabrication and oil absorption properties of superhydrophobic recycled cellulose aerogels, 168–175, Copyright 2015,with permission from Elsevier).

values of the external surface were slightly higher than those of the cross section, possibly due to the greater accessibility of the external surface.

To examine the hydrophobic stability of the cellulose aerogels, they were then exposed to the normal ambient atmosphere for five months. Their water contact angles of 145–155° over this period were examined. Interestingly, all the cellulose aerogels exhibited similar water contact angles of approximately 150°, regardless of their cellulose concentrations or Kymene amounts. It is well known that the water contact angles strongly depend on the functional groups on the aerogel surfaces. Therefore, in this case, such a small variation in the water contact angles may likely have been a consequence of the identical functional groups (–Si–O–CH_3–) induced by the MTMS coating.[40] Furthermore, the water contact angles of the cellulose aerogels on the external surface and the cross-section did not show any obvious change with time. The hydrophobic properties of the aerogels discussed in this section demonstrate the excellent performance of the MTMS coating on different types of cellulose aerogels.

14.2.3.3 Oil Absorption Properties of the Cellulose Aerogels

The oil absorption properties of the recycled cellulose aerogels are discussed in this section. Several factors, such as the type of oil, the initial cellulose fibre concentration, the temperature, and the seawater effect with different pH values, were investigated with regard to their effects on the oil absorption capacity of the cellulose aerogels. The absorption kinetics and the activation energy values of cellulose aerogels are also investigated in detail in this section.

14.2.3.3.1 Absorption Capacities with Different Oils. A 5w40 motor oil was used to investigate the oil absorption capabilities of the recycled cellulose aerogels listed in Table 14.1. This section focuses on motor oils

Table 14.1 Chemical compositions of the various recycled cellulose aerogels. (Reprinted from *Chemical Engineering Journal*, **270**, J. Feng, S. T. Nguyen, Z. Fan, H. M. Duong, Advanced fabrication and oil absorption properties of superhydrophobic recycled cellulose aerogels, 168–175, Copyright 2015, with permission from Elsevier).

Sample label	Cellulose fibres (wt.%)	Kymene (μl)	Porosity (%)
Sample A	0.25	5	99.4 ± 0.0
Sample B	0.50	5	98.9 ± 0.0
Sample C	0.75	5	98.1 ± 0.0
Sample D	1.00	5	97.2 ± 0.1
Sample E	0.60	5	98.4 ± 0.0
Sample F	0.60	20	98.4 ± 0.0
Sample G	1.00	10	97.4 ± 0.0
Sample H	2.00	20	96.9 ± 0.0
Sample I	4.00	40	96.1 ± 0.3

instead of crude oils, as it aims to show the excellent absorption properties of cellulose aerogels with oil products containing additives.

When the Kymene amount was kept at 5 μl and the cellulose concentration was increased from 0.25 to 0.50 to 0.75 to 1.00 wt.%, the measured absorption capacities of the aerogels (Samples A, B, C, and D in Table 14.1) were 95, 73, 58, and 49 $g\,g^{-1}$, respectively, at 25 °C. The maximum absorption capacity of 95 $g\,g^{-1}$ was achieved with the 0.25 wt.% cellulose aerogel, because it had the lowest density (9×10^{-3} $g\,cm^{-3}$) and the highest porosity (99.4%).

The absorption capacities of all the MTMS-coated cellulose aerogels were one order greater than those of the natural sorbents, two to ten times greater than those of the commercial polypropylene sorbents, and five times greater than those of the recycled cellulose aerogels (approximately 20 $g\,g^{-1}$) reported in previous works that used the sodium hydroxide/urea method.[11,19,25,40,41] The significant enhancement of the absorption capacity may be largely ascribed to the reduced densities and increased porosities of the cellulose aerogels.

The cellulose aerogels fabricated with a Kymene binder can achieve a high porosity (up to 99.4%), while the cellulose aerogels using sodium hydroxide and urea can achieve only 98.0% porosity. When the cellulose amounts were further decreased in the syntheses mixture using sodium hydroxide and urea, rigid aerogels could not be successfully formed.

Temperature is also a major factor affecting the viscosity and the diffusion capability of the oils into the porous aerogel structures. Therefore, the absorption behaviour of the different oils with each aerogel were examined at three different temperatures of 25, 50, and 70 °C. As shown in Table 14.2 and Figure 14.4, the maximum oil absorption capacity increased when the temperature was increased from 25 to 50 °C, but then decreased when the temperature was further increased from 50 to 70 °C. This trend holds for the absorption behaviour of all the oils with the 0.50, 0.75, and 1.00 wt.% cellulose aerogels.

The explanation for this may be that the temperature increase reduced the oil viscosities (shown in Table 14.3), which in turn facilitated oil penetration into the porous aerogel networks. However, the lower viscosities of the oils also had a negative effect on their ability to anchor to the pore walls, reducing the amounts of oil retained in the porous absorbents during drainage. Comparing the maximum oil absorption capacity with the tested temperatures, it can be concluded that 50 °C is the optimum temperature for maximizing the oil absorption performance of the recycled cellulose aerogels.

Besides the temperature effects, the porosity of cellulose aerogels also significantly affects their oil absorbency. Table 14.2 and Figure 14.4 show that the oil absorption capacity of the aerogels was reduced when the initial cellulose concentration increased from 0.50 to 1.00 wt.%. This can be explained by the porosity of the cellulose aerogels. Table 14.1 shows that the aerogel porosity reduced from 98.9 to 97.2% when the cellulose

Table 14.2 Summary of the maximum oil absorption capacities and the absorption rate constants of the cellulose aerogels at different temperatures, with various cellulose fibre concentrations, using the pseudo-first-order and pseudo-second-order models. (Reprinted from *Chemical Engineering Journal*, **270**, J. Feng, S. T. Nguyen, Z. Fan, H. M. Duong, Advanced fabrication and oil absorption properties of superhydrophobic recycled cellulose aerogels, 168–175, Copyright 2015,with permission from Elsevier).

	Cellulose concentration (wt.%)		0.50			0.75			1.00		
	Temperature (°C)		25	50	70	25	50	70	25	50	70
5w50 motor oil	Maximum absorption capacity, Q_m (g g^{-1})		62.6	64.9	59.2	48.1	53.8	46.3	45.9	46.5	46.2
	Pseudo-first-order	R^2	0.986	0.970	0.972	0.977	0.954	0.966	0.986	0.993	0.944
		K_1	0.293	0.324	0.355	0.254	0.319	0.367	0.218	0.287	0.357
	Pseudo-second-order	R^2	0.996	0.996	0.998	0.995	0.998	0.996	0.996	0.995	0.998
		K_2	0.006	0.008	0.009	0.008	0.010	0.015	0.005	0.007	0.013
Singer machine oil	Maximum absorption capacity, Q_m (g g^{-1})		59.3	61.0	58.2	46.1	48.8	47.6	40.4	43.1	42.4
	Pseudo-first-order	R^2	0.983	0.978	0.980	0.981	0.956	0.994	0.978	0.970	0.987
		K_1	0.297	0.311	0.351	0.273	0.306	0.343	0.278	0.377	0.425
	Pseudo-second-order	R^2	0.994	0.999	0.999	0.996	0.995	0.999	0.993	0.994	0.996
		K_2	0.008	0.010	0.012	0.008	0.011	0.015	0.007	0.009	0.016

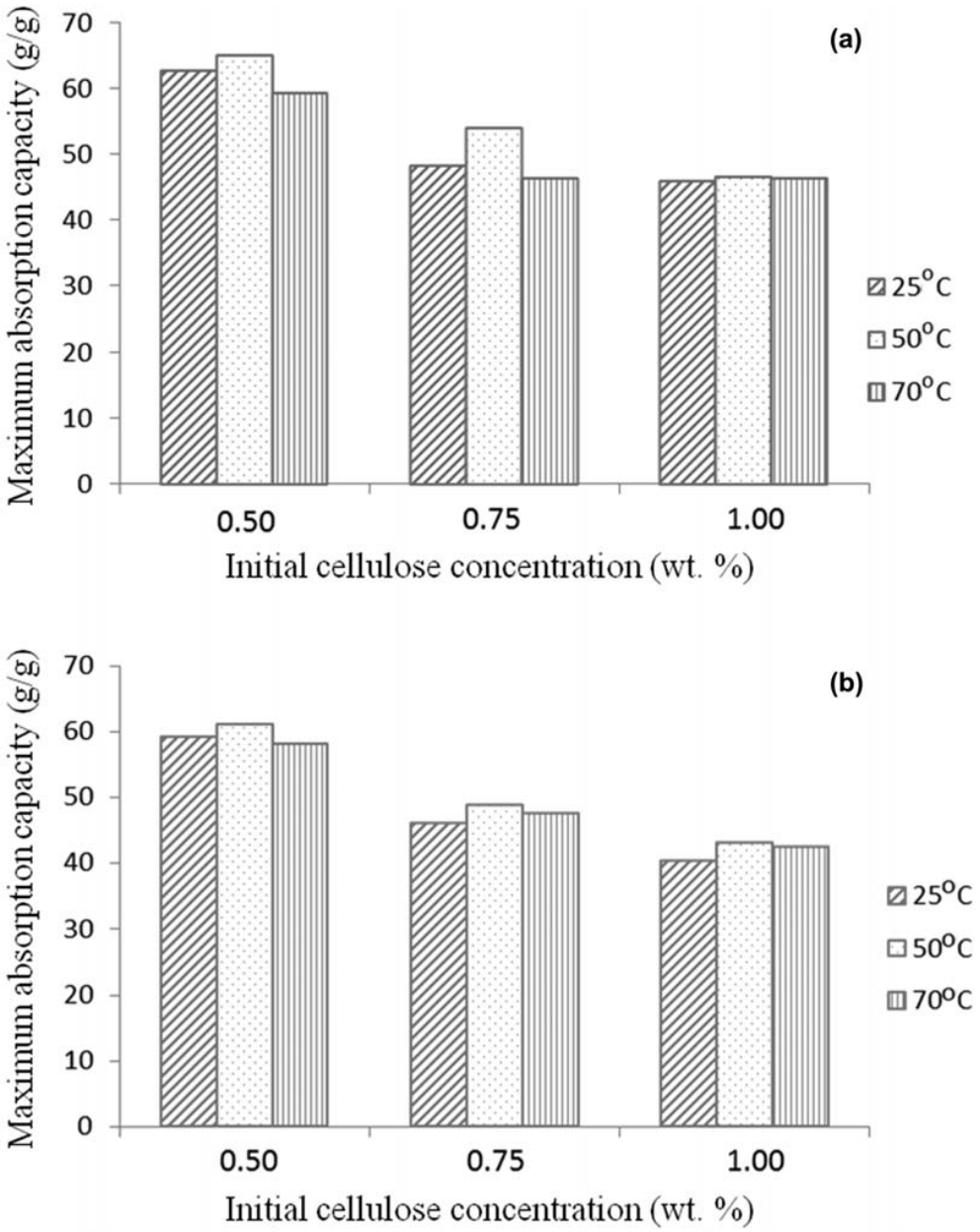

Figure 14.4 Maximum absorption capacities, Q_m, of (a) the 5w50 motor oil and (b) the Singer machine oil with the recycled cellulose aerogels with various cellulose fibre concentrations of 0.50, 0.75, and 1.00 wt.% at 25, 50, and 70 °C.
(Reprinted from *Chemical Engineering Journal*, **270**, J. Feng, S. T. Nguyen, Z. Fan, H. M. Duong, Advanced fabrication and oil absorption properties of superhydrophobic recycled cellulose aerogels, 168–175, Copyright 2015,with permission from Elsevier).

concentration increased from 0.50 to 1.00 wt.%. As the aerogel porosity was lower, there was less space in the aerogel network for oil occupation, and therefore the oil absorbency was lower.

To evaluate the practical oil absorption performance of the recycled cellulose aerogels in the sea, a 3.5% NaCl solution was prepared to imitate seawater. Figure 14.5 illustrates the absorption process over several minutes.

Table 14.3 The relevant viscosities of the tested oils at different temperatures. (Reprinted from *Chemical Engineering Journal*, **270**, J. Feng, S. T. Nguyen, Z. Fan, H. M. Duong, Advanced fabrication and oil absorption properties of superhydrophobic recycled cellulose aerogels, 168–175, Copyright 2015, with permission from Elsevier).

Viscosity (Pa.s)	25 °C	50 °C	70 °C
5w40 motor oil	0.140	n.a.	n.a.
5w50 motor oil	0.160	0.054	0.029
Singer machine oil	0.026	0.009	0.006

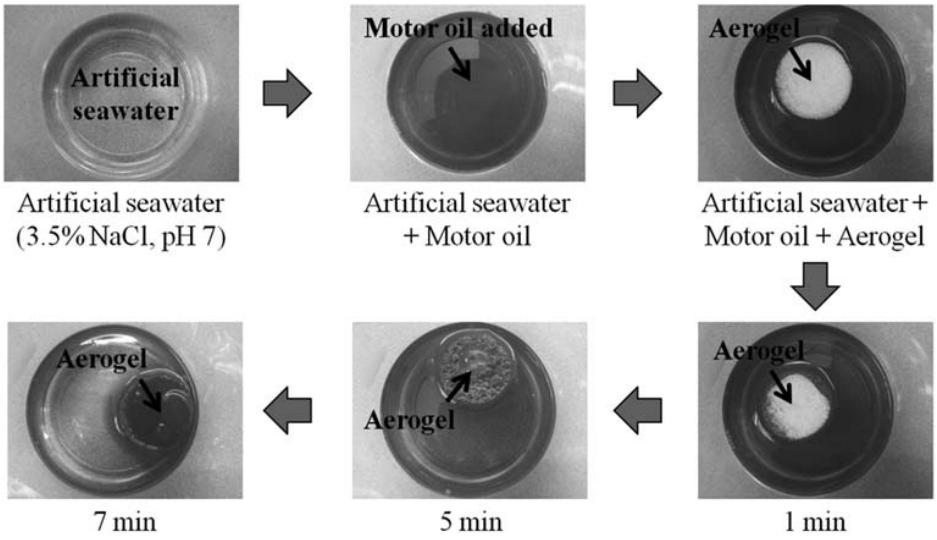

Figure 14.5 Oil absorption process of the recycled cellulose aerogel with 0.5 wt.% of cellulose fibres in artificial seawater (3.5 wt.% NaCl and pH = 7) mixed with 5w40 motor oil and dyed with Sudan Red G before testing. (Reprinted from *Chemical Engineering Journal*, **270**, J. Feng, S. T. Nguyen, Z. Fan, H. M. Duong, Advanced fabrication and oil absorption properties of superhydrophobic recycled cellulose aerogels, 168–175, Copyright 2015,with permission from Elsevier).

The cellulose aerogel was loaded on top of the mixture, and quickly absorbed most of the motor oil within 7 min.

In addition, the effects of pH on the oil absorption capacities of the cellulose aerogels were investigated using different pH values prepared from HCl or NaOH. The oil absorption capacities of the 0.50 wt.% cellulose aerogels under pH = 3, 5, 7, and 9 environments were measured to be 63.00, 62.85, 63.06, and 62.98 $g\,g^{-1}$, respectively. The absorption results indicated pH-insensitive behaviour of the aerogels during the oil absorption tests, possibly because the oil capacities of aerogels are mostly controlled by their porosities and tested oil viscosities, both of which are independent of environmental pH values.

14.2.3.3.2 Absorption Kinetics with Different Oils. The absorption kinetics of the 5w50 motor oil and Singer machine oil on recycled cellulose

aerogels were investigated, and are summarized in Table 14.2. Although sample A, with a cellulose fibre concentration of 0.25 wt.% (Table 14.1), had the highest oil absorption capacity, it possessed a less rigid structure and was easy to disintegrate after repeated draining and absorbing of oil. Therefore, three different aerogel samples, marked B, C, and D (Table 14.1) and with cellulose fibre concentrations of 0.50, 0.75, and 1.00 wt.% respectively, were prepared for the oil absorption kinetics tests at 25 °C. As shown in Figure 14.6, the sorption capacity of each oil on the cellulose aerogels was plotted as a function of absorption time. The sorption rate was fast during the first 10 s, and the absorption reached the equilibrium state at 30 s for both of the two oils.

Figure 14.7 shows the absorption kinetics[60,61] of the 5w50 motor oil and Singer machine oil on the 0.50 wt.% cellulose aerogel at 25 °C, respectively. The plots of $\ln[Q_m/(Q_m - Q_t)]$ *versus* time t using the pseudo-first-order model pseudo-second-order models yield the sorption rate constants k_1 and k_2, and the correlation coefficient R^2 are presented in Table 14.2. It can be observed that the correlation coefficient values of the pseudo-second-order model are higher than those of the pseudo-first-order model for both tested oils. Therefore, the pseudo-second-order model could better predict the oil absorption behaviour. Most of the absorption rate constants (k_1 and k_2) for the Singer oil were bigger than those for the 5w50 motor oil. In addition, the absorption rate constants at a higher temperature were larger than those of the same oil and sample at a lower temperature. These suggest the oil absorption processes of the Singer oil, and those at the higher temperature occur faster. Figures 14.7a and b show the experimental absorption kinetics data and the two fitted model curves for the absorption of the two oils on the 0.50 wt.% cellulose aerogels, which show a good agreement.[60,61] The values of k_1 and k_2 are generally much larger than those reported. This phenomenon indicates that the absorption speed of the cellulose aerogels described in this section, with 5w50 motor oil and Singer oil, were much higher than those of the cellulose aerogels described with crude oils. This may be explained by the high porosities of the cellulose aerogels.

The activation energy, E_a, is an important parameter in a thermodynamic study.[62] For example, during a successful absorption process, the activation energy must be overcome by an absorbate to interact with functional groups on the sorbent surface. The activation energy, E_a, can be determined from the change in the absorption rate constant, k, with temperature, T (K), using the Arrhenius equation:[62,63]

$$\ln k = \ln A - \frac{E_a}{RT} \tag{14.1}$$

in which A is the pre-exponential factor and R is the gas constant (8.314 J mol^{-1} K^{-1}). By plotting $\ln[k]$ against $1/T$, E_a can be calculated from the slope.

The activation energy values are presented in Table 14.4. It can be observed that the activation energy values of the pseudo-second-order model

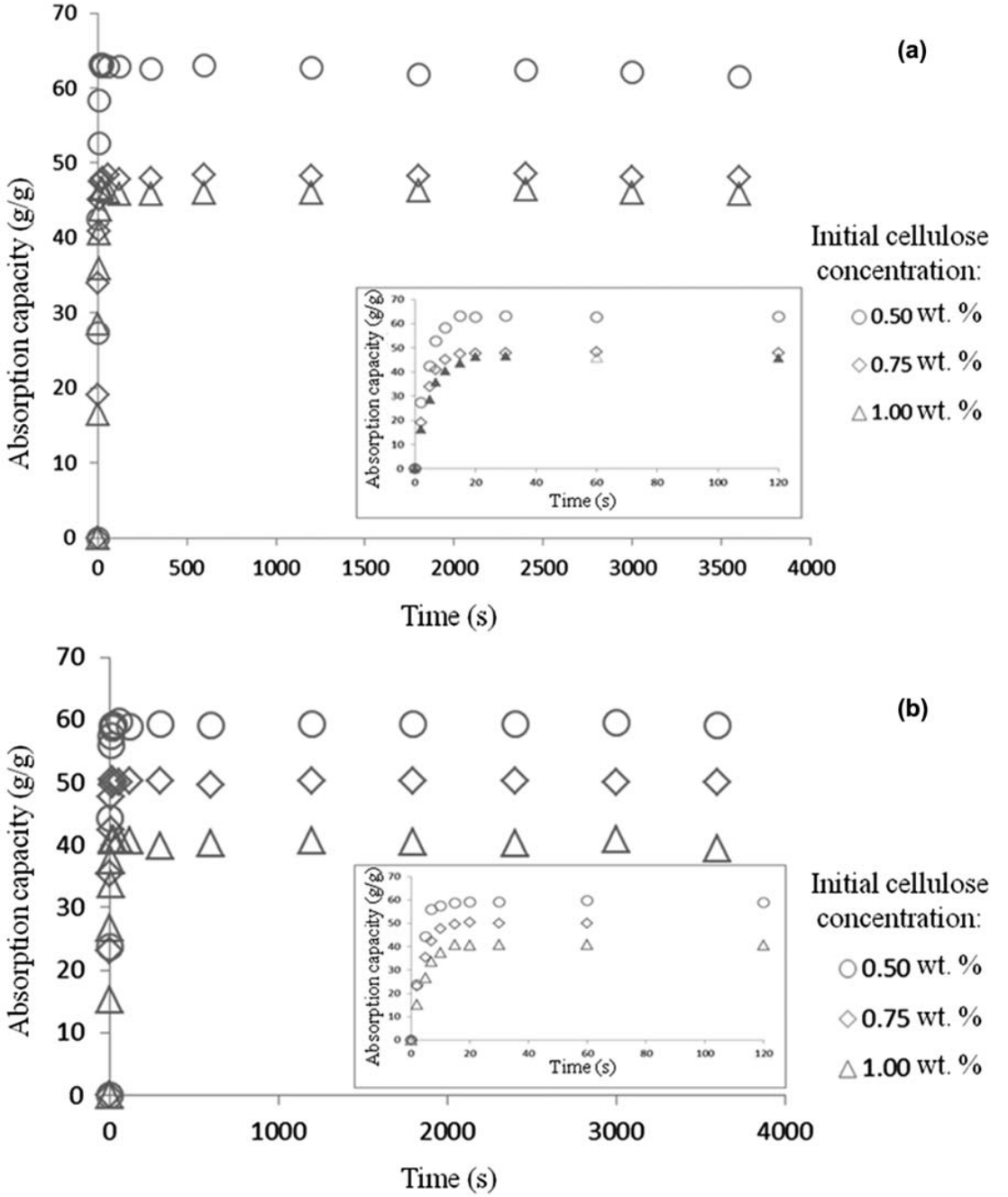

Figure 14.6 Absorption kinetics of (a) the 5w50 motor oil and (b) the Singer machine oil on the recycled cellulose aerogels with various cellulose fibre concentrations of 0.50, 0.75, and 1.00 wt.% at 25 °C. The magnified images show the absorption kinetics of the initial 2 min of the absorption processes.
(Reprinted from *Chemical Engineering Journal*, **270**, J. Feng, S. T. Nguyen, Z. Fan, H. M. Duong, Advanced fabrication and oil absorption properties of superhydrophobic recycled cellulose aerogels, 168–175, Copyright 2015,with permission from Elsevier).

are higher than those of the pseudo-first-order model. This is because the pseudo-second-order model was used for the absorption process controlled by chemi-sorption, which involves higher forces than in physic-sorption.[64]

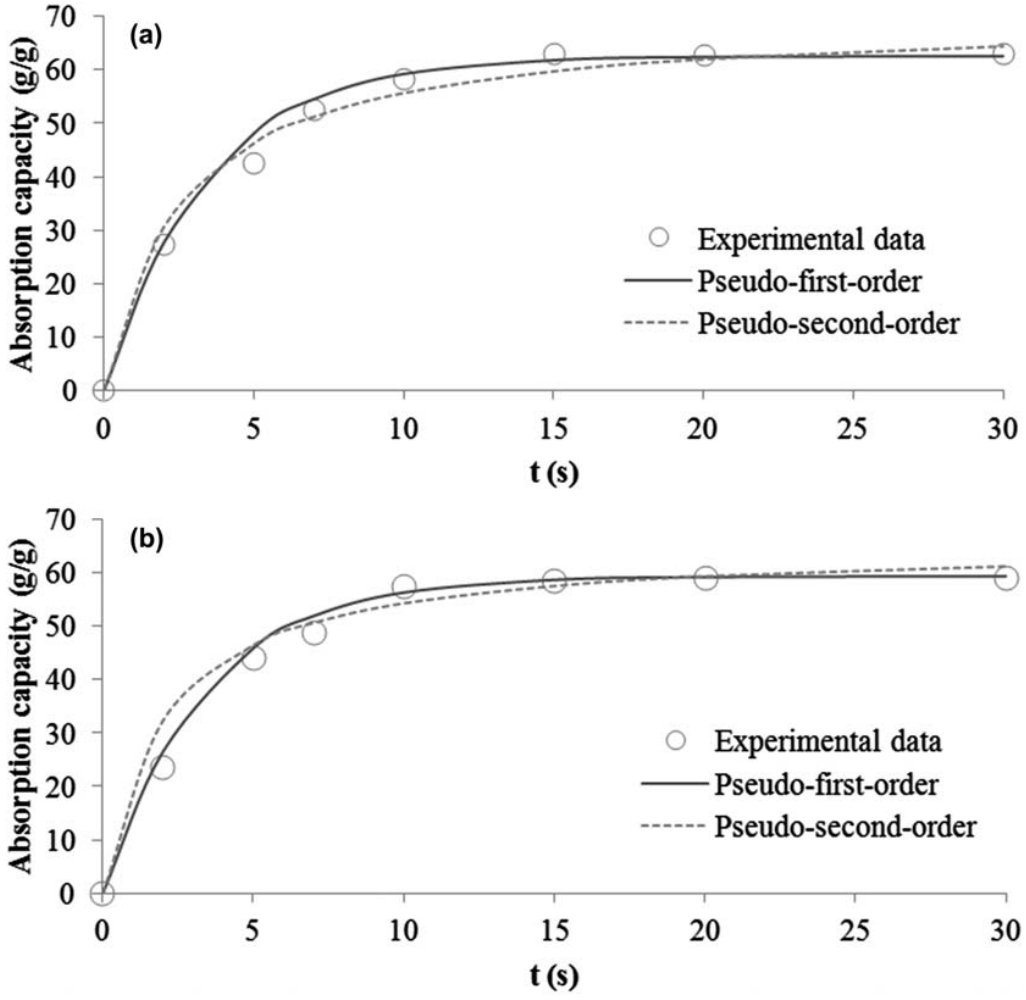

Figure 14.7 Experimental data fitted with the pseudo-first-order and pseudo-second-order models for the absorption kinetics of (a) the 5w50 motor oil and (b) the Singer machine oil on the aerogel with 0.50 wt.% of cellulose fibres at 25 °C.
(Reprinted from *Chemical Engineering Journal*, **270**, J. Feng, S. T. Nguyen, Z. Fan, H. M. Duong, Advanced fabrication and oil absorption properties of superhydrophobic recycled cellulose aerogels, 168–175, Copyright 2015,with permission from Elsevier).

Table 14.4 Activation energies of the absorption of the cellulose aerogels with various cellulose concentrations on the oils, using the pseudo-first-order and pseudo-second-order models. (Reprinted from *Chemical Engineering Journal*, **270**, J. Feng, S. T. Nguyen, Z. Fan, H. M. Duong, Advanced fabrication and oil absorption properties of superhydrophobic recycled cellulose aerogels, 168–175, Copyright 2015, with permission from Elsevier).

Activation energies ($J\,mol^{-1}$)	Initial cellulose concentration (wt.%)	0.50	0.75	1.00
5w50 motor oil	Pseudo-first-order	3609.6	6984.6	9331.6
	Pseudo-second-order	10682.7	13120.3	18612.6
Singer machine oil	Pseudo-first-order	3090.5	4248.0	8130.2
	Pseudo-second-order	9354.9	10610.3	15240.4

In addition, compared with the 5w50 motor oil, the Singer machine oil had lower activation energy values, which made the oil absorption on the cellulose aerogels more effective.

14.2.4 Summary

In conclusion, the advanced and cost-effective fabrication method of the recycled cellulose aerogels was further improved. The MTMS-coated cellulose aerogels exhibited stable hydrophobicity during a test period of over five months. Their excellent oil absorption capacities were demonstrated with motor oil and Singer oil. It was found that the initial cellulose fibre concentration significantly affected the oil absorption capability of the developed cellulose aerogels. The 0.25 wt.% cellulose aerogel yielded a maximum absorption capacity of 95 $g\,g^{-1}$ with the 5w40 motor oil. The maximum absorption capacity of the cellulose aerogels could be reached at 50 °C, regardless of the pH values of the seawater/oil suspensions, and decreased with an increase in the cellulose fibre concentration.

The pseudo-first-order and pseudo-second-order kinetics models were applied to describe the oil absorption behaviour of the recycled cellulose aerogels for the first time. The pseudo-second-order model was more suited to the oil absorption kinetics study of the aerogels, due to its chemi-sorption nature. Moreover, the recycled cellulose aerogels displayed excellent flexibility: the large-scale cellulose aerogel could be easily bent or rolled without damaging its shape. All of the tested cellulose aerogels could also be compressed to up to 70% strain. The experimental results demonstrate that the super-hydrophobic recycled cellulose aerogels could be very promising sorbents for oil-spill cleaning.

14.3 Cellulose-based Aerogels for Heat-insulation Applications

14.3.1 Introduction

The greenhouse effect is gradually warming up the earth and potentially threatening human life. It was found that CO_2 emissions from buildings contributed approximately 31% of global greenhouse-gas emissions in 2010.[65,66] Improving thermal insulation of buildings is one of the most effective solutions for this issue. Therefore, many efforts have been made to develop new insulation materials.[67] Silica aerogels have been investigated as insulation materials for buildings.[68] However, they are very brittle. A flexible, aerogel-based insulation material has been developed by Aspen Aerogels (USA), but it is much more expensive than conventional insulation materials.[68] As a result, there is considerable need for insulation materials with reasonably low thermal conductivities and costs. These materials should also have high thermal stability for fire safety.

This section focuses on the thermal properties, such as thermal conductivity and thermal stability, of the recycled cellulose aerogels and their silica composites.[69] This is the first time that the benchmark data of the thermal properties of recycled cellulose-based aerogels has been reported. Of the recycled cellulose-based materials, the recycled cellulose aerogels using sodium hydroxide–urea aqueous solutions showed the lowest thermal conductivities (0.032 $W\,mK^{-1}$); however, the cellulose aerogels display a continuous weight loss from below 100 °C, during the thermogravimetric (TGA) test. The cellulose–silica composite aerogels displayed the best thermal stability; however, their thermal conductivities (0.039–0.041 $W\,mK^{-1}$) are much higher than those of the cellulose aerogels using sodium hydroxide–urea aqueous solutions (0.032 $W\,mK^{-1}$). In summary, the recycled cellulose aerogels using a Kymene binder (the aerogels with the lowest cost), exhibit lower thermal conductivities (0.034–0.037 $W\,mK^{-1}$) than those of the composite aerogels (0.039–0.041 $W\,mK^{-1}$), and a higher thermal stability (with a decomposition temperature of approximately 300 °C) surpassing that of the cellulose aerogels using sodium hydroxide–urea aqueous solutions. The recycled cellulose aerogels are therefore the most promising thermal insulation material.

14.3.2 Synthesis of Silica–Cellulose Aerogels

The catalyst solution was prepared by mixing 10.250 g of ammonium hydroxide and 0.927 g of ammonium fluoride in 50 ml of deionised (DI) water. After that, 6 ml of MTMS solution was mixed with 11 ml of ethanol and stirred for 5 min (forming an MTMS/ethanol solution). Then, 7 ml of DI water, 11 ml of ethanol, and 0.5 ml of the catalyst solution were mixed in another beaker (forming a water/ethanol/catalyst solution). While the MTMS/ethanol mixture was still being stirred, the obtained DI water/ethanol/catalyst solution was poured slowly into the MTMS/ethanol mixture and stirred for another 15 min to form the sol. The sol was poured into a mould that contained the cellulose aerogel, and the gelation and aging process were conducted at room temperature (25 °C) for three days. After solvent exchange between the gel and DI water, the obtained hydrogel was frozen and dried using a Scan Vac CoolSafe 95-15 Pro freeze dryer (Denmark) for 24 h. Different silica–cellulose aerogels were synthesized from the different cellulose aerogel matrixes with varied cellulose fibre concentrations inside the initial cellulose aqueous suspensions. The fabrication method of pure recycle cellulose aerogel can be found in the section 14.2.2.

14.3.3 Thermal Properties of the Cellulose-based Aerogels

14.3.3.1 Thermal Properties of the Recycled Cellulose Aerogels Using a Kymene Binder

The thermal conductivities of the aerogels were measured under ambient conditions using a C-Therm TCi Thermal Conductivity Analyzer (C-Therm

Table 14.5 Effects of cellulose fibre concentrations on the thermal conductivities of the cellulose aerogels using a Kymene binder. (Reprinted from *Colloids and Surfaces A: Physicochemical and Engineering Aspects*, **506**, J. Feng, D. Le, S. T. Nguyen, V. T. C. Nien, D. Jewell, H. M. Duong, Silica cellulose hybrid aerogels for thermal and acoustic insulation applications, 298–305, Copyright 2016, with permission from Elsevier).

Cellulose fibre concentration (wt.%)	Density ($g\,cm^{-3}$)	Thermal conductivity ($W\,mK^{-1}$)
1.0	0.0392 ± 0.0005	0.0340 ± 0.0003
2.0	0.0473 ± 0.0004	0.0353 ± 0.0006
4.0	0.0592 ± 0.0032	0.0366 ± 0.0003

Technologies, Canada), with the MTPS method. Using this approach, the thermal conductivities of the recycled cellulose aerogels fabricated with a Kymene binder were measured. The porosity of the cellulose aerogels using a Kymene binder significantly affected their thermal conductivities. Table 14.5 shows that the thermal conductivity of the aerogels using a Kymene binder increased from 0.034 to 0.037 $W\,mK^{-1}$ when the initial cellulose fibre concentration increased from 1.0 to 4.0 wt.%. Increases in the initial cellulose fibre concentration led to decreases in the porosity of the resultant cellulose aerogels. When the porosity is lower, there is more solid substance to promote thermal conduction and reduce thermal insulation.

The thermal stability of the cellulose aerogels using a Kymene binder was much better than that of the cellulose aerogels fabricated from the sodium hydroxide–urea aqueous solution. A weight loss of 6.5 wt.%, corresponding to the water release, was observed in the temperature range of 25–150 °C for the cellulose aerogel using a Kymene binder. Slow decomposition of the material was observed between 150 and 300 °C, and 86.3 wt.% remained of the cellulose aerogel using a Kymene binder at 300 °C. In comparison, 40.7 wt.% remained of the cellulose aerogel fabricated from the sodium hydroxide–urea aqueous solution at the same temperature. The obvious differences suggest that the thermal stability of the cellulose aerogel using a Kymene binder was much better than that of the cellulose aerogel synthesized *via* the sodium hydroxide–urea route. The differences between the thermal stabilities of these two cellulose aerogels could possibly be explained by two major factors: (1) there was no urea involved in the fabrication of the cellulose aerogels *via* the Kymene route, and so there was no urea residue;[39] and (2) the sonication method applied with the Kymene route, as a mechanical approach, had an advantage over the chemical treatment methods regarding thermal stability of the cellulose materials.[70,71]

14.3.3.2 Thermal Properties of the Silica–Cellulose Aerogels

The silica–cellulose composite aerogels were fabricated by immersing the cellulose matrixes inside the solutions containing a silica precursor. The cellulose matrixes were the recycled cellulose aerogels (obtained after

hydrophobic coating) fabricated with a Kymene binder. The main purpose of the development of the silica–cellulose aerogels was to further improve the thermal stability and mechanical strength of the pure cellulose aerogels. The different silica–cellulose aerogels were synthesized from the varied cellulose matrixes with different initial recycled cellulose fibre concentrations (1.0–4.0 wt.%) in the initial cellulose suspensions.

14.3.3.2.1 Morphology and Hydrophobicity of the Silica–Cellulose Aerogels. The morphologies of the silica–cellulose composite aerogels were investigated with FE-SEM. Figure 14.8a–c display the SEM images of the silica–cellulose aerogels fabricated with the cellulose matrixes with different cellulose fibre concentrations in the initial cellulose aqueous suspensions. The images in Figure 14.8a–c suggest that the cellulose matrix served as the three-dimensional supporting frame.

The intersection points between the cellulose fibres were strengthened by a great number of hydrogen-bond links, which helped the formation of the strong supporting frame.[72] The strong supporting frame restricted the silica particles firmly within it by a confinement effect.[73] Meanwhile, the interconnected silica particles reinforced the cellulose matrix by attaching themselves to the matrix. As a result, a more rigid structure was formed. The structures of the silica–cellulose aerogels using different cellulose aerogel

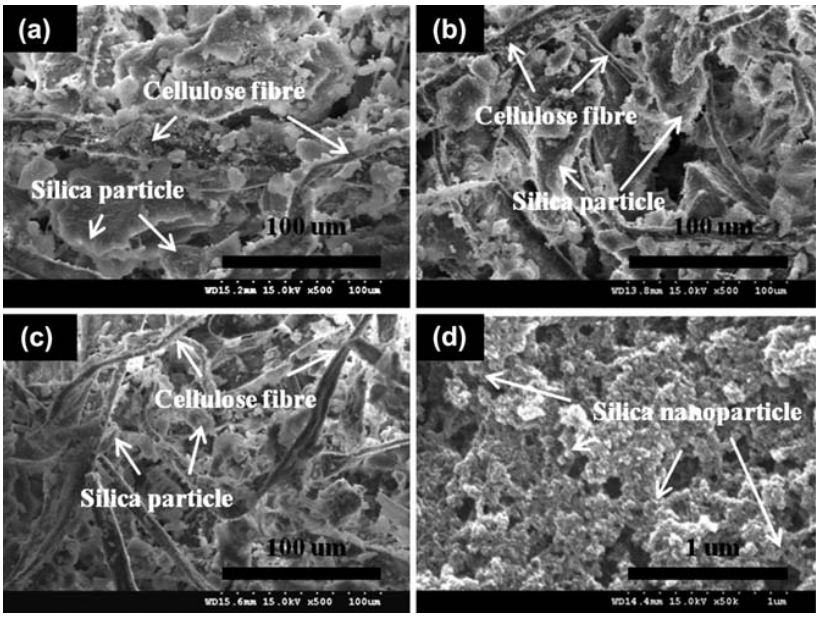

Figure 14.8 SEM images of the silica–cellulose aerogels fabricated with the cellulose matrixes with different cellulose fibre concentrations (a) 1.0 wt.%, (b) 2.0 wt.%, and (c) 4.0 wt.% in the initial cellulose aqueous suspensions. (d) A typical image of the zoomed-in silica region of the composites. (Reprinted from *Colloids and Surfaces A: Physicochemical and Engineering Aspects*, **506**, J. Feng, D. Le, S. T. Nguyen, V. T. C. Nien, D. Jewell, H. M. Duong, Silica cellulose hybrid aerogels for thermal and acoustic insulation Applications, 298–305, Copyright 2016, with permission from Elsevier).

matrixes were compared. When the cellulose content was higher, silica particles with a smaller particle size and more uniform distribution were found. This phenomenon might be explained by the following speculation. Before the freeze drying, the cellulose fibres were embedded in the silica hydrogel. During the freeze drying (including the freezing pre-treatment), the silica particles further away from the cellulose fibres experienced less force from the cellulose matrix than the silica particles next to the cellulose fibres. The denser cellulose matrix led to a more uniform distribution of small silica particles because of the more uniformly distributed force exerted by the cellulose matrix. On the other hand, the loose cellulose matrix with many large pores yielded a number of large silica particles located away from the cellulose fibres because of the small force exerted by the cellulose matrixes. At the same time, inside the loose cellulose matrix, the large silica particles located away from the cellulose fibres coexisted with the small silica particles that formed near the cellulose fibres, yielding a less uniform distribution.

The mesostructure of the silica particles was similar to the findings of other groups that developed silica–cellulose aerogels.[73,74] The BET surface areas of the silica–cellulose composite aerogels in Table 14.6 were between approximately 198 and 296 $m^2 g^{-1}$, comparable to the surface areas found in similar studies conducted by Demilecamps *et al.* (90–170 $m^2 g^{-1}$)[75] and Litschauer *et al.* (220–290 $m^2 g^{-1}$).[76]

As can be observed in Figure 14.9, the X-ray diffraction patterns of the silica–cellulose composite aerogels seem to be the superposition of those of the pure cellulose aerogels and the pure silica aerogels, which is similar to the findings of Cai *et al.*[77] This XRD finding implies that the extent of the chemical reaction between the cellulose fibres and the silica components was quite limited, as no new compound was detected. The XRD results suggest that it was reasonable for the meso-porous structure of the silica–cellulose aerogels to be controlled only by the silica components as the cellulose matrix did not possess a detectable BET surface area, and no new compound was formed. In addition, the XRD results indicate that the attachments between the cellulose fibres and the silica particles observed in the SEM images were physical instead of chemical.

According to Shi *et al.*, the hydrophobicity of the composite could improve the stability of the heat-insulation performance of the material.[74] To date, research on hydrophobic modifications of silica–cellulose composite aerogels

Table 14.6 Morphology studies of the cellulose–silica composites.

Cellulose fibre concentration inside the initial suspension for cellulose matrix fabrication (wt.%)	Density ($g\,cm^{-3}$)	SiO_2 in composite aerogel (wt.%)	BET surface area ($m^2 g^{-1}$)	Porosity (%)
1.0	0.149 ± 0.005	79 ± 4	296 ± 31	93.8 ± 0.0
2.0	0.146 ± 0.005	73 ± 5	248 ± 28	93.8 ± 0.0
4.0	0.138 ± 0.002	60 ± 3	198 ± 24	93.7 ± 0.0

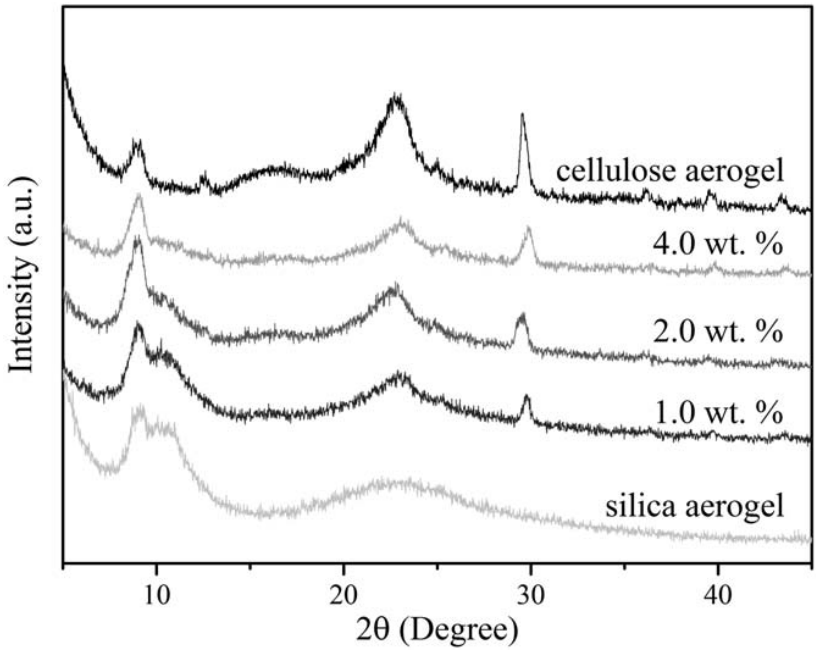

Figure 14.9 XRD patterns of the silica aerogel, the cellulose aerogel, and the silica–cellulose aerogels fabricated from cellulose matrixes with different cellulose fibre concentrations (1.0, 2.0, and 4.0 wt.%) inside the initial suspensions.
(Reprinted from *Colloids and Surfaces A: Physicochemical and Engineering Aspects*, **506**, J. Feng, D. Le, S. T. Nguyen, V. T. C. Nien, D. Jewell, H. M. Duong, Silica cellulose hybrid aerogels for thermal and acoustic insulation Applications, 298–305, Copyright 2016, with permission from Elsevier).

has been limited. In 2013, Shi *et al.* applied a CCl_4 cold-plasma modification approach using gas ionization.[74] In the same year, Sai *et al.* proposed a solvent-immersion method involving a 24 h aging followed by freeze drying.[73] Both methods might be considered uneconomical because of either the expensive equipment or the large amount of chemicals and the long duration involved. Moreover, the water contact angles of the modified composite aerogels from the above two methods were similar (132° and 133°), indicating that the aerogels were not super-hydrophobic.[73,74] However, the silica–cellulose composite aerogels exhibited super-hydrophobic properties. The average water contact angle was approximately 151° for all three composites. The excellent water-repelling property of the composites was inherited from both the hydrophobic cellulose matrix and the silica precursor (MTMS). Meanwhile, the stable methyl group of MTMS was responsible for the excellent hydrophobicity of the silica components.[78] Further modification of the fabricated composite aerogels was not required to achieve the superhydrophobicity, which could be considered a remarkable advantage.

14.3.3.2.2 Thermal Conductivity of the Silica–Cellulose Aerogels. The thermal conductivities of the silica–cellulose aerogels (0.0385–0.0410 $W\,mK^{-1}$) increase with the increase in density (0.138–0.149 $g\,cm^{-3}$). With references to Table 14.5 and Table 14.7, the thermal conductivities and the densities of

Table 14.7 The thermal conductivities of the silica–cellulose aerogels fabricated from cellulose matrixes with different cellulose fibre concentrations in the initial suspensions. (Reprinted from *Colloids and Surfaces A: Physicochemical and Engineering Aspects*, **506**, J. Feng, D. Le, S. T. Nguyen, V. T. C. Nien, D. Jewell, H. M. Duong, Silica cellulose hybrid aerogels for thermal and acoustic insulation Applications, 298–305, Copyright 2016, with permission from Elsevier).

Cellulose fibre concentration in the initial suspension for cellulose-matrix fabrication (wt.%)	Density ($g\,cm^{-3}$)	Thermal conductivity ($W\,mK^{-1}$)
1.0	0.149 ± 0.005	0.0410 ± 0.0003
2.0	0.146 ± 0.005	0.0390 ± 0.0006
4.0	0.138 ± 0.002	0.0387 ± 0.0003

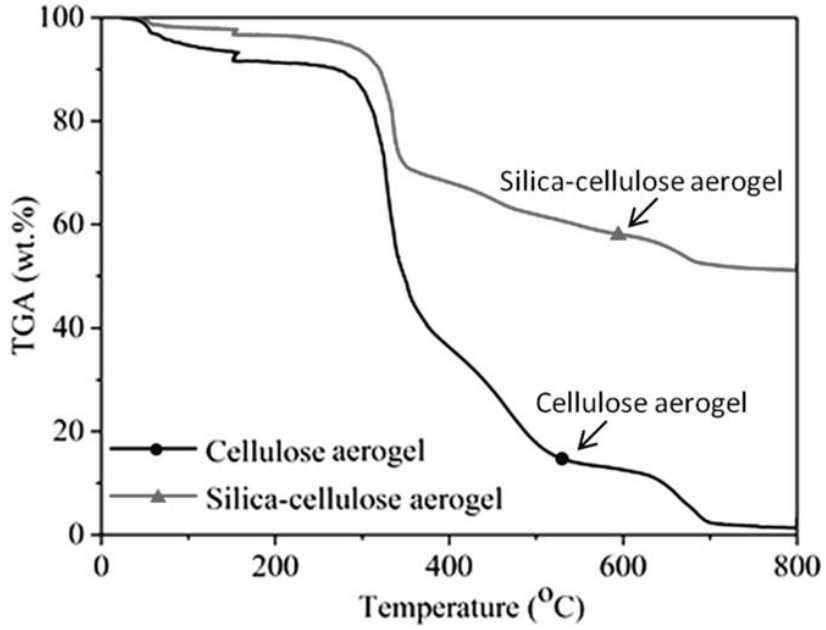

Figure 14.10 The thermogravimetric analysis (TGA) curve of the silica–cellulose aerogel, compared with that of the cellulose aerogel using a Kymene binder. The composite aerogels were fabricated from cellulose matrixes with different cellulose fibre concentration of 4.0 wt.% in the initial suspensions.

the silica–cellulose aerogels (0.0385–0.0410 $W\,mK^{-1}$; 0.138–0.149 $g\,cm^{-3}$) were higher than those of the cellulose aerogels using a Kymene binder (0.034–0.037 $W\,mK^{-1}$; 0.039–0.059 $g\,cm^{-3}$). One possible reason is that the thermal conductivities increase with density.[79,80] The thermal conductivities of the silica–cellulose aerogels (0.0385–0.0410 $W\,mK^{-1}$) were lower than those of the silica–cellulose composites fabricated by other groups (0.15 $W\,mK^{-1}$), and comparable to those of conventional insulation materials, such as polyurethane foams (0.02–0.04 $W\,mK^{-1}$) and insulation boards (0.035–0.16 $W\,mK^{-1}$).[81]

As shown in Figure 14.10, it is clear that the thermal stability of the composite was better than that of the pure cellulose aerogel without the silica

embedment. A small weight loss of approximately 2 wt.% of the composites before 150 °C corresponds to the water release. The cellulose aerogel using a Kymene binder showed an approximately 7 wt.% weight loss up to 150 °C, which is greater than that of the composite. This smaller weight loss from the desorbed water was due to the super-hydrophobicity of the composite.

A 25 °C delay in the thermal degradation of the cellulose component of the composite was observed at 325 °C, compared with 300 °C before the silica modification. This increase in the degradation temperature might have been due to an interaction between the silica and the cellulose matrix at higher temperatures, and the interaction showed a positive effect on the thermal resistance of the composite.[81,82] At 300 °C, 93 wt.% silica–cellulose aerogels remained, as opposed to 86 wt.% of cellulose aerogels using the Kymene binder, demonstrating a better thermal stability. The slow mass loss of the residual substances, followed the rapid oxidative decomposition stage, after which the oxidation of the charred residue occurred and continued to the plateau. At the plateau, 51 wt.% of the silica–cellulose aerogel was preserved, mainly containing the silica.

14.3.3.2.3 Mechanical Properties of the Silica–Cellulose Aerogels. The silica modification did not impede the ductile behaviour of the silica–cellulose aerogels. The compressive strain–stress curves of the silica–cellulose aerogels fabricated from different cellulose matrixes are displayed in Figure 14.11.

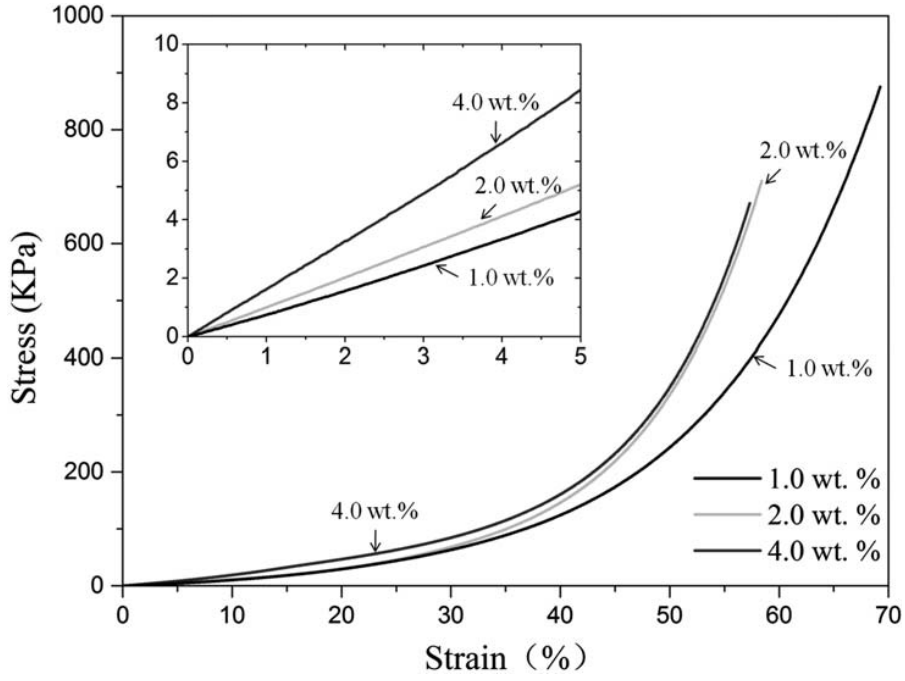

Figure 14.11 The compressive strain–stress curves of the silica–cellulose aerogels fabricated from the cellulose matrixes with different cellulose fibre concentrations (1.0, 2.0, and 4.0 wt.%) in the initial suspensions. The magnified section shows the compressive curves at the low strain (up to 5%) for the composite aerogels.

Table 14.8 The Young's modulus of the silica–cellulose composites and their cellulose aerogel matrixes. (Reprinted from Reference [69] with permission from Elsevier).

Cellulose fibre concentration in the initial suspension for cellulose matrix fabrication (wt.%)	Young's modulus of cellulose matrix (KPa)	Density of composite ($g\,cm^{-3}$)	Young's modulus of composite (KPa)
1.0	13 ± 1	0.149 ± 0.005	86 ± 3
2.0	21 ± 1	0.146 ± 0.005	104 ± 3
4.0	39 ± 2	0.138 ± 0.002	169 ± 5

Silica embedment improved the mechanical strength of the aerogels dramatically. The compressive Young's moduli of the composites were three to five times greater than those of their cellulose aerogel matrixes, as shown in Table 14.8. One contributing factor to the high mechanical strength of the silica–cellulose aerogels was their high densities compared with those of the cellulose matrixes, which is typical for many material systems, as the materials are more rigid and stiff, with a higher density.[83,84] From a microcosmic aspect, the silica particles restrained the bending of the cellulose fibres, improving the mechanical strength of the silica–cellulose aerogels.

For the silica–cellulose aerogels, the Young's modulus increased with slight decreases in density, as suggested in Table 14.8. This might possibly be explained by the increased cellulose content of the silica–cellulose aerogels. The cellulose matrix reinforces and constrains the silica granules, and the higher cellulose content leads to a more rigid cellulose matrix; thus the Young's modulus of the composite increases with the increase in the cellulose content.

14.3.4 Summary

In summary, the three recycled cellulose-based aerogels with three different thermal property combinations have been discussed. The thermal conductivity of the cellulose aerogel using a sodium hydroxide–urea aqueous solution was 0.032 $W\,mK^{-1}$, which was the lowest among the recycled cellulose fibre-based aerogels. However, the cellulose content of this material begins to degrade at 150 °C; therefore the material will require substantial modifications if the thermal stability is a major concern.

The recycled cellulose aerogels using a Kymene binder with cost-effective fabrication displayed better thermal stability than the cellulose aerogels using a sodium hydroxide–urea aqueous solution. However, the thermal conductivities of the aerogels using a Kymene binder were between 0.034 and 0.037 $W\,mK^{-1}$. These thermal conductivity values are slightly higher than those of the cellulose aerogels using a sodium hydroxide–urea aqueous solution.

To improve the thermal stability of the recycled cellulose-based aerogels further, the silica–cellulose composite aerogels were successfully developed.

A 25 °C delay in the cellulose degradation was also observed for the composites. The developed silica–cellulose aerogels also had better mechanical strengths (compressive Young's modulus: 86–169 KPa) than those of the cellulose aerogels (compressive Young's modulus: 13–39 KPa). Moreover, the inherent super-hydrophobic property of the silica–cellulose aerogels is also desirable for reliable and long-term thermal insulation. The thermal conductivities of the silica–cellulose aerogels were approximately 0.04 $W\,mK^{-1}$, comparable to those of commercial insulation products and lower than those of the cellulose aerogels.

14.4 Protein-based Aerogels and Their Applications

Recently, natural protein-based aerogels have attracted increasing research interest due to their biocompatibility and biodegradability for food engineering and life science applications. A few proteins such as whey protein,[43–45] silk fibroin,[46,47] egg white protein,[48] and soy protein[49–52] have been exploited for the formation of aerogels. This section introduces the fabrication methods and the multi-properties of the different types of protein-based aerogels and their potential applications.

14.4.1 Whey Protein Aerogels

Whey protein is the collection of globular proteins isolated from whey, which is the liquid remaining after milk has been curdled and strained for cheese production. This protein is typically a mixture of beta-lactoglobulin, alpha-lactalbumin, bovine serum albumin and immunoglobulins.[85] Whey protein is widely used in the food industry applications including processed meats, bakery products, pasta, ice cream, and infant foods.[44,86] As a by-product of the manufacture of cheese or casein, the broad availability in western countries makes whey protein promising for environmentally friendly-materials.[44]

Betz *et al.* developed a novel whey protein-based aerogel for drug delivery applications.[43] Previous studies indicated that the water-insoluble whey protein hydrogels were applicable for the encapsulation of drugs.[87,88] The use of supercritical drying and freeze drying techniques resulted in the drying of covalently crosslinked hydrogels and generated a highly porous aerogel. The obtained mechanically stable aerogels possessed a high BET-surface area (310–388 $m^2\,g^{-1}$) and drug loading capacity (9.1–9.5%, w/w for ketoprofen). The covalent disulphide bonds avoided the collapse of the aerogel structure when placed in the presence of aqueous media and led to a pH-controlled swelling behaviour upon rehydration. Due to the water-insolubility of the whey protein aerogels, the drug-loaded aerogels showed a sustained drug release at gastric (pH 1.2) and intestinal (pH 6.8) simulated digestive pH conditions. Later, Chen *et al.* prepared whey protein aerogels with enhanced mechanical properties.[44] By blending with alginate, the compressive moduli of the obtained aerogels were significantly enhanced by

crosslinking and further increased with increasing aerogel densities. Ahmadi *et al.* prepared whey protein aerogels blended with nanocrystalline and microcrystalline cellulose particles and achieved increased Young's modulus and elastic character of the aerogels.[45] It was found that the nanocrystalline and microcrystalline cellulose particles impacted the texture of whey protein aerogels to different extents. Blending with cellulose nanocrystalline particles reinforced the texture of protein aerogels and decreased the sub-100 nm pore volume. The obtained protein aerogels were further applied for fish oil encapsulation.

14.4.2 Silk Fibroin Aerogels

Silk fibroin is a natural protein, derived from the Bombyx mori silkworm. Due to their biocompatibility and biodegradability, silk fibroin based porous materials have been extensively investigated for biomedical applications.[47] Marin *et al.* developed silk fibroin aerogels as drug delivery devices for the extended release of ibuprofen, a candidate drug.[46] Ibuprofen, a candidate drug compound, was loaded into the silk fibroin aerogels using supercritical CO_2. The obtained aerogels demonstrated high surface areas of $424 \pm 75\ m^2\,g^{-1}$ and low densities of $0.058 \pm 0.001\ g\,ml^{-1}$. Phosphate buffer solution soaking studies revealed that the silk fibroin aerogels did not swell, nor exhibited any weight loss for up to 6 h. Release of ibuprofen from SF aerogels was found to be governed by Fickian diffusion.

Later, Mallepally *et al.* applied silk fibroin aerogels as potential scaffolds for tissue engineering applications.[47] Silk fibroin aerogel scaffolds were successfully fabricated using sol–gel and supercritical CO_2 processing protocols. The morphology and textural properties of the silk fibroin aerogels could be tuned by the starting concentration of the silk fibroin aqueous solution. When the aqueous fibroin concentration increased from 2 to 6 wt.%, the surface area of the resultant aerogels increased from 260 to $308\ m^2\,g^{-1}$ and the compressive modulus increased from 19.5 to 174 kPa. Silk fibroin cryogels were also synthesised, in order to study the effect of hydrogels pretreatments on the morphological and textural properties.[47] The silk fibroin aerogels demonstrated a surface area of $266\ m^2\,g^{-1}$ and pore volume of $1.6\ cc\,g^{-1}$, which was significantly higher compared to the freeze-dried silk fibroin cryogels with a surface area of $45\ m^2\,g^{-1}$ and pore volume of $0.05\ cc\,g^{-1}$. These results make these silk fibroin aerogels promising for cell culture and tissue engineering applications. *In vitro* cell culture studies with human foreskin fibroblast cells showed that the silk fibroin aerogels were cytocompatible with human cells and the aerogel scaffold promoted their propagation.

14.4.3 Egg White Protein Aerogels

As a high quality protein source with high nutrition, egg white protein offers versatile functional properties and it is widely used in the food industry.[89]

Native egg white consists of about 10 wt.% protein and 90 wt.% water.[89] When egg white is heated, the egg white proteins denature thermally and form a gel whose structure is influenced by pH, ionic strength and the type of added salt.[90] Selmer *et al.* developed egg white protein-based aerogels as a carrier material for food applications.[48] The aerogels were prepared by gelation of pasteurized and spray-dried egg white solutions and subsequent supercritical drying. The porosity and surface area of the aerogels could be tailored by controlling the pH and ionic strength of the solution during the gelation process. The largest BET-surface area of 380 $m^2 g^{-1}$ was achieved at pH 2, while the most mechanically stable aerogels were obtained at alkaline pH. In order to produce mechanically stable aerogels with high surface areas, pH values above the isoelectrical point should be used. These protein-based aerogels were suitable as microencapsulation materials for sensitive or unpleasant tasting food additives.

14.4.4 Soy Protein Aerogels

Soy flour, as a great source of protein, contains approximately 42% protein, 20% oil, 33% carbohydrates, and 5% ash on a dry basis. Protein from soy is mainly composed of acidic amino acids such as aspartic and glutamic acids, non-polar amino acids (glycine, alanine, valine and leucine), basic amino acids (lysine and arginine), and less than 1% of cysteine.[91] The soy protein-based aerogels have been designed for different applications.[49–52] Amaral-Labat *et al.* reported the first natural organic aerogels at the 91% level, which were prepared from gelation of tannin–soy flour resin in aqueous solution, followed by supercritical drying in CO_2.[49] The resultant aerogels presented a low density of 0.19–0.25 $g\,cm^{-3}$ and high mesopore volumes up to 2.3 $cm^3 g^{-1}$. The pore structures of the aerogels were tuneable by varying the pH values in the synthesis processes. These soy–tannin aerogels have potential for various applications, such as catalyst supports, adsorption of acidic species in liquids or natural super-insulators.

To improve the mechanical properties of the soy protein aerogels, Arboleda *et al.* developed the soy protein–nanocellulose composite aerogels.[50] The nanofibrillar cellulose loading resulted in the morphology transition of the aerogels from network- to fibrillar-like, with a high density of interconnected cells. With soy protein loadings as high as ca. 70%, the aerogels showed a high compression modulus of 4.4 MPa. The developed aerogels can absorb water and other solvents while maintaining their integrity. Due to their low density and good mechanical properties, these soy protein based aerogels are interesting candidates for applications including packaging, thermal and acoustic insulation, and so forth.

14.5 Conclusions

Paper waste can be successfully converted into cellulose-based aerogels with high oil absorption capacities (95 $g\,g^{-1}$), good thermal-insulation

performances (0.032 $W\,mK^{-1}$), and excellent water-repellent properties (151°). Recycled cellulose-based aerogels utilizing paper waste are promising and economical candidates for several applications, such as oil-spill cleaning and building thermal insulation. In addition, morphology control of the recycled cellulose aerogels could be efficiently achieved by changing the cellulose concentration. To obtain the hydrophobic coating, a simple but effective chemical vapour deposition method *via* MTMS was developed, and the stability of the hydrophobic coating was tested. The recycled cellulose aerogels generated from both fabrication methods demonstrated stable hydrophobic properties over the tested time span of five months.

The initial cellulose fibre concentration played a critical role in the absorption capacities: the decreases in the initial cellulose fibre concentration led to increases in the absorption capacities due to the reduced porosities. The optimum temperature for high oil absorption capacity was 50 °C (of 25, 50, and 70 °C) because of the favourable viscosities of the oils at this temperature, as the viscosities were low enough for the oils to efficiently penetrate the porous aerogel networks, and high enough for the oils to effectively anchor to the pore walls of the cellulose aerogels. In addition, the pH values of the seawater/oil suspension had negligible effects on the oil absorption capacities of the cellulose aerogels, as the key factors affecting absorption capacity (the porosities of the cellulose aerogels and the viscosities of the oils) were independent of the environmental pH values.

The most cost-effective cellulose aerogels using a Kymene binder showed an observable improvement in thermal stability over the previous cellulose aerogels, because the Kymene method mainly applies a mechanical approach and no urea is involved. To improve the thermal stability further, the silica–cellulose aerogels were successfully developed. The major DTA peak also shifted from 352 °C for the cellulose aerogels to 530–550 °C for the silica–cellulose aerogels, as the major DTA peak of the composites is caused by the oxidation of the methyl group of the silica component. In addition, the silica–cellulose aerogels displayed an inherent super-hydrophobic property and better mechanical strength (Young's modulus: 86–169 KPa) than the cellulose aerogels using a Kymene binder (4–39 KPa). However, the thermal conductivities (approximately 0.04 $W\,mK^{-1}$) of the silica–cellulose aerogels were higher than those of the cellulose aerogels using a Kymene binder, due to their high density and low porosity.

Protein-based aerogels are novel biodegradable and biocompatible materials for lightweight food engineering and life science applications. The types of proteins, initial protein concentrations, processing techniques and many environmental conditions demonstrate significant influences on the structures and properties of the resultant aerogels. Further studies are required to tailor the morphological and textural properties of these protein-based aerogels with enhanced mechanical stability for practical applications.

References

1. O. A. Centeno-Chalé, M. L. Aguirre-Macedo, G. Gold-Bouchot and V. M. Vidal-Martínez, Effects of Oil Spill Related Chemical Pollution on Helminth Parasites in Mexican Flounder Cyclopsetta Chittendeni from the Campeche Sound, Gulf of Mexico, *Ecotoxicol. Environ. Saf.*, 2015, **119**, 162–169.
2. D. Li, F. Z. Zhu, J. Y. Li, P. Na and N. Wang, Preparation and Characterization of Cellulose Fibers from Corn Straw as Natural Oil Sorbents, *Ind. Eng. Chem. Res.*, 2012, **52**(1), 516–524.
3. H. Li, L. Liu and F. Yang, Hydrophobic Modification of Polyurethane Foam for Oil Spill Cleanup, *Mar. Pollut. Bull.*, 2012, **64**(8), 1648–1653.
4. V. Singh, R. J. Kendall, K. Hake and S. Ramkumar, Crude Oil Sorption by Raw Cotton, *Ind. Eng. Chem. Res.*, 2013, **52**(18), 6277–6281.
5. J. Wang, Y. Zheng, Y. Kang and A. Wang, Investigation of Oil Sorption Capability of Pbma/Sio 2 Coated Kapok Fiber, *Chem. Eng. J.*, 2013, **223**, 632–637.
6. N. Xiao, Y. Zhou, Z. Ling and J. Qiu, Synthesis of a Carbon Nanofiber/Carbon Foam Composite from Coal Liquefaction Residue for the Separation of Oil and Water, *Carbon*, 2013, **59**, 530–536.
7. K. Zhu, Y.-Y. Shang, P.-Z. Sun, Z. Li, X.-M. Li and J.-Q. Wei *et al.*, Oil Spill Cleanup from Sea Water by Carbon Nanotube Sponges, *Front. Mater. Sci.*, 2013, 7(2), 170–176.
8. Q. Zhu, Y. Chu, Z. Wang, N. Chen, L. Lin and F. Liu *et al.*, Robust Superhydrophobic Polyurethane Sponge as a Highly Reusable Oil-Absorption Material, *J. Mater. Chem. A*, 2013, **1**(17), 5386–5393.
9. D. Cormack, B. Lynch and B. Dowsett, Evaluation of Dispersant Effectiveness, *Oil Chem. Pollut.*, 1986, **3**(2), 87–103.
10. M. F. Fingas, R. Stoodley and N. Laroche, Effectiveness Testing of Spill-Treating Agents, *Oil Chem. Pollut.*, 1990, **7**(4), 337–348.
11. A. Bayat, S. F. Aghamiri, A. Moheb and G. R. Vakili-Nezhaad, Oil Spill Cleanup from Sea Water by Sorbent Materials, *Chem. Eng. Technol.*, 2005, **28**(12), 1525–1528.
12. R. M. Atlas, Petroleum Biodegradation and Oil Spill Bioremediation, *Mar. Pollut. Bull.*, , **31**(4), 178–182.
13. D. Dave and A. E. Ghaly, Remediation Technologies for Marine Oil Spills: A Critical Review and Comparative Analysis, *Am. J. Environ. Sci.*, 2011, **7**(5), 423.
14. A. A. Al-Majed, A. R. Adebayo, M. E. Hossain and A. Sustainable, Approach to Controlling Oil Spills, *J. Environ. Manage.*, 2012, **113**, 213–227.
15. Y. Chu and Q. Pan, Three-Dimensionally Macroporous Fe/C Nanocomposites as Highly Selective Oil-Absorption Materials, *ACS Appl. Mater. Interfaces*, 2012, **4**(5), 2420–2425.
16. C. Cojocaru, M. Macoveanu and I. Cretescu, Peat-Based Sorbents for the Removal of Oil Spills from Water Surface: Application of Artificial Neural Network Modeling, *Colloids Surf., A*, 2011, **384**(1), 675–684.

17. X. Gui, H. Li, K. Wang, J. Wei, Y. Jia and Z. Li *et al.*, Recyclable Carbon Nanotube Sponges for Oil Absorption, *Acta Mater.*, 2011, **59**(12), 4798–4804.
18. X. Gui, Z. Zeng, Z. Lin, Q. Gan, R. Xiang and Y. Zhu *et al.*, Magnetic and Highly Recyclable Macroporous Carbon Nanotubes for Spilled Oil Sorption and Separation, *ACS Appl. Mater. Interfaces*, 2013, **5**(12), 5845–5850.
19. M. O. Adebajo, R. L. Frost, J. T. Kloprogge, O. Carmody and S. Kokot, Porous Materials for Oil Spill Cleanup: A Review of Synthesis and Absorbing Properties, *J. Porous Mater.*, 2003, **10**(3), 159–170.
20. D. Peng, Z. Lan, C. Guo, C. Yang and Z. Dang, Application of Cellulase for the Modification of Corn Stalk: Leading to Oil Sorption, *Bioresour. Technol.*, 2013, **137**, 414–418.
21. D. Bastani, A. Safekordi, A. Alihosseini and V. Taghikhani, Study of Oil Sorption by Expanded Perlite at 298.15 K, *Sep. Purif. Technol.*, 2006, **52**(2), 295–300.
22. O. Karakasi and A. Moutsatsou, Surface Modification of High Calcium Fly Ash for Its Application in Oil Spill Clean Up, *Fuel*, 2010, **89**(12), 3966–3970.
23. V. Rajakovic, G. Aleksic, M. Radetic and L. Rajakovic, Efficiency of Oil Removal from Real Wastewater with Different Sorbent Materials, *J. Hazard. Mater.*, 2007, **143**(1), 494–499.
24. G. Deschamps, H. Caruel, M.-E. Borredon, C. Bonnin and C. Vignoles, Oil Removal from Water by Selective Sorption on Hydrophobic Cotton Fibers. 1. Study of Sorption Properties and Comparison with Other Cotton Fiber-Based Sorbents, *Environ. Sci. Technol.*, 2003, **37**(5), 1013–1015.
25. R. Wahi, L. A. Chuah, T. S. Y. Choong, Z. Ngaini and M. M. Nourouzi, Oil Removal from Aqueous State by Natural Fibrous Sorbent: An Overview, *Sep. Purif. Technol.*, 2013, **113**, 51–63.
26. X. Yuan and T. M. Chung, Novel Solution to Oil Spill Recovery: Using Thermodegradable Polyolefin Oil Superabsorbent Polymer (Oil–Sap), *Energy Fuels*, 2012, **26**(8), 4896–4902.
27. N. T. Cervin, C. Aulin, P. T. Larsson and L. Wågberg, Ultra Porous Nanocellulose Aerogels as Separation Medium for Mixtures of Oil/Water Liquids, *Cellulose*, 2012, **19**(2), 401–410.
28. J. T. Korhonen, M. Kettunen, R. H. Ras and O. Ikkala, Hydrophobic Nanocellulose Aerogels as Floating, Sustainable, Reusable, and Recyclable Oil Absorbents, *ACS Appl. Mater. Interfaces*, 2011, **3**(6), 1813–1816.
29. K. C. Payne, C. D. Jackson, C. E. Aizpurua, O. J. Rojas and M. A. Hubbe, Oil Spills Abatement: Factors Affecting Oil Uptake by Cellulosic Fibers, *Environ. Sci. Technol.*, 2012, **46**(14), 7725–7730.
30. J. Wang, Y. Zheng and A. Wang, Effect of Kapok Fiber Treated with Various Solvents on Oil Absorbency, *Ind. Crops Prod.*, 2012, **40**, 178–184.
31. J. Wang, Y. Zheng and A. Wang, Coated Kapok Fiber for Removal of Spilled Oil, *Mar. Pollut. Bull.*, 2013, **69**(1), 91–96.

32. A. Nourbakhsh and A. Ashori, Particleboard Made from Waste Paper Treated with Maleic Anhydride, *Waste Manage. Res.*, 2010, **28**(1), 51–55.
33. L. Szabó, A. Soria, J. Forsström, J. T. Keränen and E. Hytönen, A World Model of the Pulp and Paper Industry: Demand, Energy Consumption and Emission Scenarios to 2030, *Environ. Sci. Policy*, 2009, **12**(3), 257–269.
34. Paper Recycling, Available from http://Www.Epa.Gov/Osw/Conserve/Materials/Paper/Basic_Info.Htm.
35. D. Mishra and V. K. Sinha, Value-Based Polymer Precursors from Paper Waste and Its Application in Polyurethane Foams, *J. Cell. Plast.*, 2009.
36. L. Wang, R. Templer and R. J. Murphy, High-Solids Loading Enzymatic Hydrolysis of Waste Papers for Biofuel Production, *Appl. Energy*, 2012, **99**, 23–31.
37. Y. Ikeda, E. Y. Park and N. Okuda, Bioconversion of Waste Office Paper to Gluconic Acid in a Turbine Blade Reactor by the Filamentous Fungus Aspergillus Niger, *Bioresour. Technol.*, 2006, **97**(8), 1030–1035.
38. The Paper Stock Report: Paper Recycling Online, Available from http://Www.Recycle.Cc/Freepapr.Htm, 2015.
39. J. Feng, S. T. Nguyen, Z. Fan and H. M. Duong, Advanced Fabrication and Oil Absorption Properties of Super-Hydrophobic Recycled Cellulose Aerogels, *Chem. Eng. J.*, 2015, **270**, 168–175.
40. S. T. Nguyen, J. Feng, N. T. Le, A. T. Le, N. Hoang and V. B. Tan *et al.*, Cellulose Aerogel from Paper Waste for Crude Oil Spill Cleaning, *Ind. Eng. Chem. Res.*, 2013, **52**(51), 18386–18391.
41. S. T. Nguyen, J. Feng, S. K. Ng, J. P. Wong, V. B. Tan and H. M. Duong, Advanced Thermal Insulation and Absorption Properties of Recycled Cellulose Aerogels, *Colloids Surf., A*, 2014, **445**, 128–134.
42. L. Heath and W. Thielemans, Cellulose Nanowhisker Aerogels, *Green Chem.*, 2010, **12**(8), 1448–1453.
43. M. Betz, C. García-González, R. Subrahmanyam, I. Smirnova and U. Kulozik, Preparation of Novel Whey Protein-Based Aerogels as Drug Carriers for Life Science Applications, *J. Supercrit. Fluids*, 2012, **72**, 111–119.
44. H.-B. Chen, Y.-Z. Wang and D. A. Schiraldi, Foam-Like Materials Based on Whey Protein Isolate, *Eur. Polym. J.*, 2013, **49**(10), 3387–3391.
45. M. Ahmadi, A. Madadlou and A. A. Saboury, Whey Protein Aerogel as Blended with Cellulose Crystalline Particles or Loaded with Fish Oil, *Food Chem.*, 2016, **196**, 1016–1022.
46. M. A. Marin, R. R. Mallepally and M. A. McHugh, Silk Fibroin Aerogels for Drug Delivery Applications, *J. Supercrit. Fluids*, 2014, **91**, 84–89.
47. R. R. Mallepally, M. A. Marin, V. Surampudi, B. Subia, R. R. Rao and S. C. Kundu *et al.*, Silk Fibroin Aerogels: Potential Scaffolds for Tissue Engineering Applications, *Biomed. Mater.*, 2015, **10**(3), 035002.
48. I. Selmer, C. Kleemann, U. Kulozik, S. Heinrich and I. Smirnova, Development of Egg White Protein Aerogels as New Matrix Material for Microencapsulation in Food, *J. Supercrit. Fluids*, 2015, **106**, 42–49.

49. G. Amaral-Labat, L. Grishechko, A. Szczurek, V. Fierro, A. Pizzi and B. Kuznetsov *et al.*, Highly Mesoporous Organic Aerogels Derived from Soy and Tannin, *Green Chem.*, 2012, **14**(11), 3099–3106.
50. J. C. Arboleda, M. Hughes, L. A. Lucia, J. Laine, K. Ekman and O. J. Rojas, Soy Protein–Nanocellulose Composite Aerogels, *Cellulose*, 2013, **20**(5), 2417–2426.
51. L. Sun, W. Chen, Y. Liu, J. Li and H. Yu, Soy Protein Isolate/Cellulose Nanofiber Complex Gels as Fat Substitutes: Rheological and Textural Properties and Extent of Cream Imitation, *Cellulose*, 2015, **22**(4), 2619–2627.
52. Y. Zhuang, F. Yu, J. Ma and J. Chen, Facile Synthesis of Three-Dimensional Graphene–Soy Protein Aerogel Composites for Tetracycline Adsorption, *Desalin. Water Treat.*, 2016, **57**(20), 9510–9519.
53. S. Hoepfner, L. Ratke and B. Milow, Synthesis and Characterisation of Nanofibrillar Cellulose Aerogels, *Cellulose*, 2008, **15**(1), 121–129.
54. N. Isobe, S. Kimura, M. Wada and S. Kuga, Mechanism of Cellulose Gelation from Aqueous Alkali-Urea Solution, *Carbohydr. Polym.*, 2012, **89**(4), 1298–1300.
55. J. Cai and L. Zhang, Unique Gelation Behavior of Cellulose in Naoh/Urea Aqueous Solution, *Biomacromolecules*, 2006, **7**(1), 183–189.
56. V. Stannett. Mechanisms of Wet-Strength Development in Paper. Surfaces and Coatings Related to Paper and Wood: A Symposium [held At] State University College of Forestry at Syracuse University: Syracuse University Press Syracuse, NY; pp. 269–300.
57. J. Cai, S. Kimura, M. Wada, S. Kuga and L. Zhang, Cellulose Aerogels from Aqueous Alkali Hydroxide–Urea Solution, *ChemSusChem*, 2008, **1**(1–2), 149–154.
58. W. Chen, H. Yu, Q. Li, Y. Liu and J. Li, Ultralight and Highly Flexible Aerogels with Long Cellulose I Nanofibers, *Soft Matter*, 2011, **7**(21), 10360–10368.
59. R. T. Olsson, M. A. Samir, G. Salazar-Alvarez, L. Belova, V. Ström and L. A. Berglund *et al.*, Making Flexible Magnetic Aerogels and Stiff Magnetic Nanopaper Using Cellulose Nanofibrils as Templates, *Nat. Nanotechnol.*, 2010, **5**(8), 584–588.
60. Y. Chen and D. Zhang, Adsorption Kinetics, Isotherm and Thermodynamics Studies of Flavones from Vaccinium Bracteatum Thunb Leaves on Nka-2 Resin, *Chem. Eng. J.*, 2014, **254**, 579–585.
61. B. Wu and M. Zhou, Recycling of Waste Tyre Rubber into Oil Absorbent, *Waste Manage.*, 2009, **29**(1), 355–359.
62. P. Saha and S. Chowdhury. Insight into Adsorption Thermodynamics: INTECH Open Access Publisher; 2011.
63. P. Sharma, B. K. Saikia and M. R. Das, Removal of Methyl Green Dye Molecule from Aqueous System Using Reduced Graphene Oxide as an Efficient Adsorbent: Kinetics, Isotherm and Thermodynamic Parameters, *Colloids Surf., A*, 2014, **457**, 125–133.
64. A. M. Vargas, A. L. Cazetta, M. H. Kunita, T. L. Silva and V. C. Almeida, Adsorption of Methylene Blue on Activated Carbon Produced from

Flamboyant Pods (Delonix Regia): Study of Adsorption Isotherms and Kinetic Models, *Chem. Eng. J.*, 2011, **168**(2), 722–730.
65. S. D. L. R. du Can, L. Price and T. Zwickel, Understanding the Full Climate Change Impact of Energy Consumption and Mitigation at the End-Use Level: A Proposed Methodology for Allocating Indirect Carbon Dioxide Emissions, *Appl. Energy*, 2015, **159**, 548–559.
66. I. P. O. C. Change. Climate Change 2014: Mitigation of Climate Change: Cambridge University Press; 2015.
67. B. P. Jelle, Traditional, State-of-the-Art and Future Thermal Building Insulation Materials and Solutions–Properties, Requirements and Possibilities, *Energy Build.*, 2011, **43**(10), 2549–2563.
68. R. Baetens, B. P. Jelle and A. Gustavsen, Aerogel Insulation for Building Applications: A State-of-the-Art Review, *Energy Build.*, 2011, **43**(4), 761–769.
69. J. Feng, D. Le, S. T. Nguyen, V. T. C. Nien, D. Jewell and H. M. Duong, Silica-Cellulose Hybrid Aerogels for Thermal and Acoustic Insulation Applications, *Colloids Surf., A*, 2016, **506**, 298–305.
70. S. Cho, Y. Choi, D. Park, S. Heo, D. Kim and H. Jin, Cellulose Nanocrystals with High Thermal Stability and Their Nanocomposites with Poly (Lactic Acid), *Int. Conf. Compos. Mater.*, 3–46.
AQ:3
71. G. Tonoli, E. Teixeira, A. Corrêa, J. Marconcini, L. Caixeta and M. Pereira-da-Silva *et al.*, Cellulose Micro/Nanofibres from Eucalyptus Kraft Pulp: Preparation and Properties, *Carbohydr. Polym.*, 2012, **89**(1), 80–88.
72. D. Klemm, B. Heublein, H. P. Fink and A. Bohn, Cellulose: Fascinating Biopolymer and Sustainable Raw Material, *Angew. Chem., Int. Ed.*, 2005, **44**(22), 3358–3393.
73. H. Sai, L. Xing, J. Xiang, L. Cui, J. Jiao and C. Zhao *et al.*, Flexible Aerogels Based on an Interpenetrating Network of Bacterial Cellulose and Silica by a Non-Supercritical Drying Process, J. Mater. Chem. *A*, 2013, **1**(27), 7963–7970.
74. J. Shi, L. Lu, W. Guo, J. Zhang and Y. Cao, Heat Insulation Performance, Mechanics and Hydrophobic Modification of Cellulose–Sio 2 Composite Aerogels, *Carbohydr. Polym.*, 2013, **98**(1), 282–289.
75. A. Demilecamps, G. Reichenauer, A. Rigacci and T. Budtova, Cellulose–Silica Composite Aerogels from ''One-Pot'' Synthesis, *Cellulose*, 2014, **21**(4), 2625–2636.
76. M. Litschauer, M.-A. Neouze, E. Haimer, U. Henniges, A. Potthast and T. Rosenau *et al.*, Silica Modified Cellulosic Aerogels, *Cellulose*, 2011, **18**(1), 143–149.
77. J. Cai, S. Liu, J. Feng, S. Kimura, M. Wada and S. Kuga *et al.*, Cellulose–Silica Nanocomposite Aerogels by in Situ Formation of Silica in Cellulose Gel, *Angew. Chem.*, 2012, **124**(9), 2118–2121.
78. A. V. Rao, M. M. Kulkarni, D. Amalnerkar and T. Seth, Superhydrophobic Silica Aerogels Based on Methyltrimethoxysilane Precursor, *J. Non-Cryst. Solids*, 2003, **330**(1), 187–195.

79. H. Simmler, S. Brunner, U. Heinemann, H. Schwab, K. Kumaran and P. Mukhopadhyaya *et al.* Vacuum Insulation Panels. Study on Vip-Components and Panels for Service Life Prediction of Vip in Building Applications (Subtask a). *Final report for the IEA/ECBCS Annex*. 2005;39.
80. M. Kiran, A. Nandanwar, M. V. Naidu and K. C. V. Rajulu, Effect of Density on Thermal Conductivity of Bamboo Mat Board, *Int. J. Agric. Forestry*, 2012, **2**(5), 257–261.
81. S. Sequeira and D. V. Evtuguin, I. Portugal. Preparation and Properties of Cellulose/Silica Hybrid Composites, *Polym. Compos.*, 2009, **30**(9), 1275–1282.
82. N. Jia, S.-M. Li, M.-G. Ma, J.-F. Zhu and R.-C. Sun, Synthesis and Characterization of Cellulose-Silica Composite Fiber in Ethanol/Water Mixed Solvents, *BioResources*, 2011, **6**(2), 1186–1195.
83. K. E. Parmenter and F. Milstein, Mechanical Properties of Silica Aerogels, *J. Non-Cryst. Solids*, 1998, **223**(3), 179–189.
84. A. H. Alaoui, T. Woignier, G. W. Scherer and J. Phalippou, Comparison between Flexural and Uniaxial Compression Tests to Measure the Elastic Modulus of Silica Aerogel, *J. Non-Cryst. Solids*, 2008, **354**(40), 4556–4561.
85. A. Haug, A. T. Høstmark and O. M. Harstad, Bovine Milk in Human Nutrition–a Review, *Lipids Health Dis.*, 2007, **6**(1), 25.
86. S. M. Fitzsimons, D. M. Mulvihill and E. R. Morris, Co-Gels of Whey Protein Isolate with Crosslinked Waxy Maize Starch: Analysis of Solvent Partition and Phase Structure by Polymer Blending Laws, *Food Hydrocolloids*, 2008, **22**(3), 468–484.
87. M. Betz and U. Kulozik, Whey Protein Gels for the Entrapment of Bioactive Anthocyanins from Bilberry Extract, *Int. Dairy J.*, 2011, **21**(9), 703–710.
88. S. Gunasekaran, L. Xiao and M. Ould Eleya, Whey Protein Concentrate Hydrogels as Bioactive Carriers, *J. Appl. Polym. Sci.*, 2006, **99**(5), 2470–2476.
89. Y. Mine, Recent Advances in the Understanding of Egg White Protein Functionality, *Trends Food Sci. Technol.*, 1995, **6**(7), 225–232.
90. T. Croguennec, F. Nau and G. Brule, Influence of Ph and Salts on Egg White Gelation, *J. Food Sci.*, 2002, **67**(2), 608–614.
91. J.-M. Raquez, M. Deléglise, M.-F. Lacrampe and P. Krawczak, Thermosetting (Bio) Materials Derived from Renewable Resources: A Critical Review, *Prog. Polym. Sci.*, 2010, **35**(4), 487–509.